IEEE Access
Multidisciplinary | Rapid Review | Open Access Journal

Received November 15, 2020, accepted December 19, 2020, date of publication December 25, 2020,
date of current version January 6, 2021.

Digital Object Identifier 10.1109/ACCESS.2020.3047429

Segmentation of Liver Lesions Without Contrast Agents With Radiomics-Guided Densely UNet-Nested GAN

XIAOJIAO XIAO[1], YAN QIANG[1], JUANJUAN ZHAO[1], XINGYU YANG[1], AND XIAOTANG YANG[2]
[1]College of Information and Computer, Taiyuan University of Technology, Taiyuan 030000, China
[2]Department of Radiology, Shanxi Province Cancer Hospital, Taiyuan 030000, China

Corresponding author: Juanjuan Zhao (zhaojuanjuan@tyut.edu.cn)

This work was supported in part by the National Natural Science Foundation of China under Grant 61872261 and Grant 61972274, in part by the Open Funding Project of State Key Laboratory of Virtual Reality Technology and Systems, Beihang University, under Grant 2018-VRLAB2018B07, and in part by the Research Project Supported by Natural Science Foundation of Shanxi Province under Grant 201801D121139.

ABSTRACT Segmentation of liver lesions on non-contrast magnetic resonance imaging (MRI) is critical for patient management and treatment planning. In clinical treatment, the imaging process suffers from high-risk, expensive, and time-consuming due to using contrast agents (CA). Furthermore, manual segmentation has the disadvantages of tedious, low-reproducibility, and high misdiagnosis rate. Although some deep-learning based works have attempted for liver lesions segmentation, they are all limited to the use of contrast-enhanced MRI. To avoid the limitations comes from CA, we proposed a Radiomics-guided Densely-UNet-Nested Generative Adversarial Networks (Radiomics-guided DUN-GAN) for automatic segmentation of liver lesions on non-contrast MRI. Radiomics-guided DUN-GAN includes a DUN segmentor and a Radiomics-guided discriminator. It uses radiomics feature of the multi-phase contrast image as prior knowledge to guide the extraction of key implicit contrast radiomics (ICR) features in non-contrast images, thus achieving the direct lesions segmentation without CA for the first time. In the DUN segmentor, an innovative nested structure of Densely-UNet-connection reliably completes the segmentation. The nested structure extracts global features, semantic features, and ICR features by reasonably sharing features and maximizing information flow. Those features are fused with a new direction strategy of multi-integration features to improve the segmentation ability. In the innovative Radiomics-guided discriminator, the radiomics feature combined with the semantic feature enhances the discrimination of Radiomics-guided discriminator. Moreover, it guides the segmentor for multiple feature extraction via using the adversarial mechanism. Radiomics-guided DUN-GAN learns the mapping relationship between images, extracting the key ICR in the non-contrast image, and finally completing the accurate segmentation. Radiomics-guided DUN-GAN obtained the Dice Similarity Coefficient results of 93.47±0.83% for the segmentation of lesions in non-contrast images from 250 clinical subjects. The results verify the Radiomics-guided DUN-GAN is accurate and robust, and it has the possibility of becoming a safe, inexpensive, and time-saving medical assistant tool in clinical diagnosis.

INDEX TERMS Liver lesions, segmentation, radiomics-feature, multi-phase non-contrast MRI, GAN.

I. INTRODUCTION

Segmentation of the liver lesions is essential for patient management and treatment planning. 1) The segmentation guides physician to make preoperative planning, which can effectively improve the success rate of lesions resection and the survival rate of patients [1]. 2) The quantitative assessment of segmentation (e.g. volume, centroid, diameter) helps physicians develop a treatment plan and predict patient survival. [2]. 3) The segmentation is considered comprehensively with the patient's age, clinical symptoms and disease severity to guide the patient's post-operative treatment to prevent further liver failure. Meantime, clinical segmentation is obtained by experienced radiologist through

The associate editor coordinating the review of this manuscript and approving it for publication was Huazhu Fu.

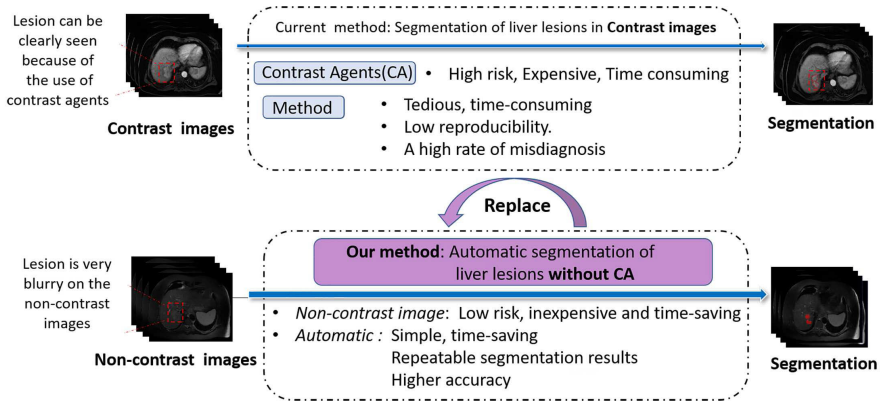

FIGURE 1. Our method directs segmentation of lesions without CA. The current methods are based on segmentation of dynamic contrast-enhanced (DCE) images, and clinical methods rely on the expertise of physician.

a visual examination. However, there are many constraints by tedious, low-reproducibility and high misdiagnosis rate in this approach (as shown in Fig. 1). Contrast agents (CA) has many potential hazards after injection into the body, even though it as chemical agents that clears the boundaries of the lesion to help segmentation [3] (as shown in Fig. 1). 1) The use of CA has a potential of high risk. The CA after injection remains in the tissue in some form (about 1% of the injected dose), which may cause potential harm because itself is potentially toxic [4]. Even more, it may trigger an incidence of 10%-15% of contrast-induced nephropathy (CIN) [5]. 2) The use of CA presents an expensive problem. The scanning cost of the Dynamic Contrast-Enhanced Magnetic Resonance Imaging(DCE-MRI) image is high. If errors occur during injection, CA materials will be wasted. 3) The use of CA has a problem with time-consumption. Injection of the CA costs additional patient time, and enhancement of the imaging process itself requires variety of imaging techniques, so it requires longer imaging waiting time. Therefore, the segmentation of non-contrast image has become a clinically urgent need for patients with liver-related diseases, especially those with impaired kidney function.

It is a great challenge to segment the lesions from the non-contrast MRI image directly, and no one has tried so far, even though there are many methods to successfully achieve segmentation of liver lesions in DCE-MRI (contrast MRI) image. 1) The lesions is almost invisible in non-contrast image, and even if it can be seen, it is a blurry border, which makes it impossible for doctors to perform accurate manual segmentation [6]. 2) The size, shape and position of lesions vary from person to person, with vast differences and complexity, resulting in a high rate of misdiagnosis. 3) Lesions are characterized by low contrast with surrounding tissues [7], different types of contrast levels (high/low intensity lesions), heterogeneous density and various shapes.

The segmentation in non-contrast images is feasible in other closer fields, such as cardiac field. Xu *et al.* [8] proposed simultaneous segmentation and quantification of myocardial infarction (MI) without contrast agents. MI can be seen in the contrast-enhanced image, but it is invisible in non-contrast images. In the MRI image sequence without CA, Xu utilizes 2D+t method to capture temporal motion features, which is a key feature of the motion of each pixel. A motion pattern of each pixel on the myocardium is established on key features to delineate the infarction area from MR images without CA accurately. However, the method does not solve the segmentation of the liver without CA in the absence of temporal motion features in the static image.

Radiomics feature [9] on the DCE-MRI images has the same potential for locating lesions as the temporal motion features. The Radiomics feature, which characterizes the potential micro-structure and heterogeneity of tumors, has a favorable performance in decoding tumors, but invisible in non-contrast images. And, multi-phase MR imaging has different information to promise for characterization of precursor lesions [7]. Critical contrast-enhanced phases include the arterial, portal venous(PV), and delay phases. Therefore, the Radiomics feature of multi-phase DCE-MRI images can guide the extraction of implicit contrast radiomics (ICR) features in non-contrast images. Adversarial learning achieves just it. This is defined as a Radiomics-guided adversarial mechanism.

We proposed a Radiomics-guided Densely-UNet-Nested (DUN) Generation Adversarial Network (Radiomics-guided DUN-GAN) for automatic segmentation of liver lesions without CA. Under the guidance of the innovative Radiomics-guided adversarial mechanism, Radiomics-guided DUN-GAN inputs the visible Radiomics feature of the multi-phase DEC-MRI(T1-Delay, T1-Arterial and T1-PV) image as guided prior knowledge to the discriminator. The guided-feature is integrated with semantic features through a Radiomics-guided connection layer (RgCL) to improve discriminating power. Moreover, it guides segmentation through adversarial learning. Segmentation is achieved through an innovative structure of Densely-UNet-Nested. This structure accurately extracts and shares global and semantic features in

the non-contrast image by expanding the receptive field and changing the information flow. All features form fusion features with enhanced characterization capabilities through an innovative direction strategy of multi-integration feature. The fusion features are utilized by Radiomics-guided DUN-GAN to extract key ICR features for accurate segmentation of lesions without CA.

This study has advances over our preliminary study in MICCAI 2019 conference [10], which provided a single-phase Radiomics-guided GAN to achieve automatic segmentation of liver lesions in non-contrast images for the first time. This study contributions and advantages of our method are as follows:

- The newly proposed multi-phase radiomics-guided mechanism successfully added multi-phase DCE-MRI to discriminator as prior knowledge. It provides an innovative adversarial mechanism of multi-phase radiomics-guide. The mechanism innovatively combined the three-phase DCE-MRI and non-contrast MRI via an adversarial mechanism for the first time, which more conducive to the feature extraction of ICR.
- A new direction strategy of multi-integration feature is designed to effectively fuse multiple features. It uses three strategies, Radiomics-guided connection layer (RgCL), global attention map guidance layer and D-connection, to integrate different features reasonably and efficiently. Integrated features take advantage of the specific information of the Radiomics-guided feature, advanced information of the global-compensate feature and deep information of the semantic feature, which have a stronger learning ability to improve the accuracy and speeds up rate of the segmentation.
- Global attention model newly added into the generator in the manner of global-guided improve DUN-generator to extract ICR better, which improves the performance of tumor segmentation. And, it integrates with other features through an integrated strategy of feature-related to reduce runtime.

Besides, the newly proposed pixel-level guided hybrid loss function can make the network converge faster and smoother. And, this study also adds more statistical verification, detailed experimental analysis, and rigorous discussion.

II. RELATED WORK

A. HAND-CRAFTED FEATURE-BASED METHODS

In existing researches, there are many successful interactive and automated methods of segmentation of liver lesions based on hand-crafted feature. The common first-type method is based on the statistical shape model [11]and some form of deformation, which was extremely successful in the challenge of liver disease segmentation at the 2008 MICCAI conference. Besides, methods based on gray level and texture have been developed. Another-type method introduces different interaction methods to guide segmentation, such as based on graphical cuts [12], [13], region-based threshold method [14], level set [15]–[17], B-spline [18] and machine learning method. 1)Region-based segmentation algorithms [19], [20] mostly use the similarity of features within the same region for image processing. For example, Sethi *et al.* [19] segment cancerous regions by selecting appropriate thresholds for different images. Region growing method extract connected regions from images by growing according to pre-defined criteria. It makes up for the lack of spatial relationship that threshold segmentation does not or seldom consider. For example, Baazaoui *et al.* [21] proposed an entropy-based fuzzy region growing method to segment single or multiple liver cancer lesions. 2) The level set method has been gradually applied to liver segmentation due to its advantages of involving numerical calculation of curves and surfaces [22]. Amarajothi *et al.* [23] combines shape and intensity prior knowledge with level set model to achieve more accurate segmentation of hepatocellular carcinoma. 3) Machine learning has gradually attracted the attention of researchers. Huang *et al.* [24] proposed an extreme learning machine (ELM) based on random feature subspace set for liver lesion segmentation. 4) There is also a combination of various methods. Zhang *et al.* [25] preprocessed the image by image enhancement and watershed transformation and trained it by support vector machine (SVM). Similarly, Kuo *et al.* [26] proposed an SVM classifier with texture feature vectors for liver lesion segmentation.

The method based on hand-crafted features can achieve better segmentation results. However, the method depends on the prior knowledge of the algorithm in the process of segmentation, such as selecting the appropriate threshold, seed points in the region growth, the number of features of machine learning, and limited expressive power when dealing with large changes in appearance and shape, which directly affects the segmentation results. In practical application, the speed and robustness of the method have not met the clinical requirements due to the limitation of low-contrast real data. Therefore, there is an urgent need for an automatic segmentation method that does not depend on hand-crafted features.

B. DEEP LEARNING-BASED METHODS

Convolutional Neural Networks (CNNs), as one of the representatives of deep learning, has completely changed the natural image processing by utilizing its highly representative features of hierarchical learning([27]–[29]), and have witnessed the successful application in the field of medical image analysis([30]–[33]). Many researchers follow this trend and propose using various CNNs to learn the feature representation in liver and lesion segmentation applications. For example, Ben-Cohen [34] proposed using FCN for liver segmentation and liver metastasis detection in CT examination.

Deep learning methods have become an alternative and crucial branch of traditional segmentation of liver lesion. It is divided into three categories. 1) Traditional 2D model, such as Cascaded-FCN [35], FCN based on VGG-16 [34]. Sun [36] designed a multi-channel FCN to segment liver

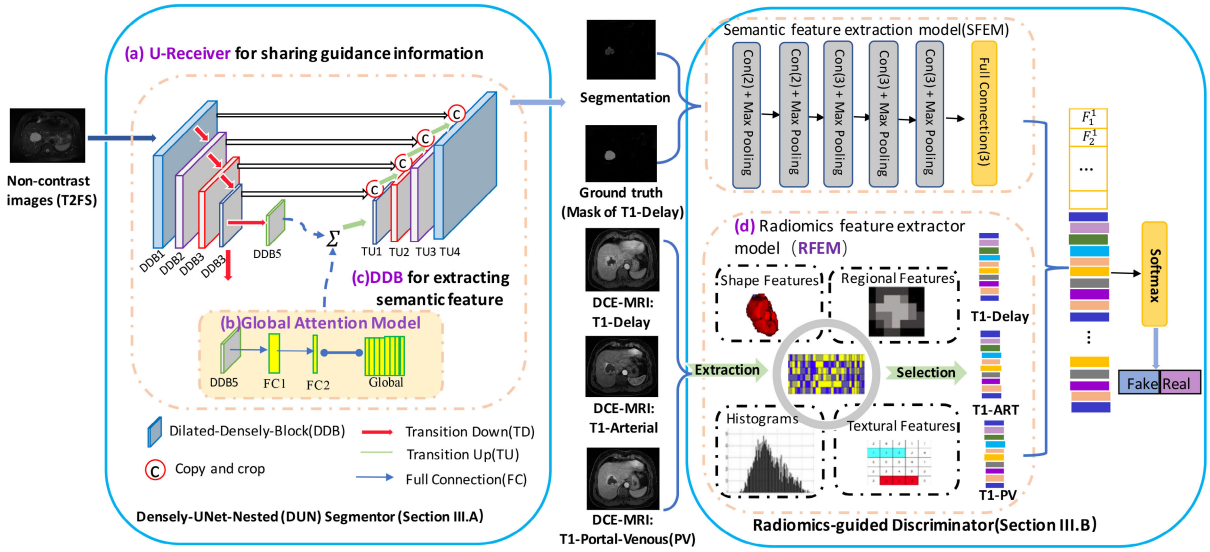

FIGURE 2. The structure of our Radiomics-guided DUN-GAN, which consists of three innovations. 1) An innovative nested system of Densely-UNet-connection is created in the Densely-UNet-Connection (DUN) segmentor. 2) A new integrated strategy of feature-related to integrate multiple features to form fusion features that can aid in the extraction of ICR features. 3) An innovative adversarial mechanism of Radiomics-guided is proposed in the Radiomics-guided discriminator.

lesions from CT images, in which probability maps are generated by feature fusion from different channels. 2) 2.5D model, such as the UNet [37] of residual connections, utilizing the similarity between slices [38]. 2.5D refers to the use of 2D convolution neural network and input from adjacent slices of volume images. During the ISBI LiTS challenge in 2017, Han [37] proposed a 2.5D FCN-24 model to segment liver lesions, in which residual blocks were used as repetitive building blocks, and UNet connections were designed throughout the coding and decoding parts. 3) 3D model, such as 3D FCN [39], densely connected volume ConvNets [40], H-DenseUnet [41], SynSeg-Net [42], and Tripartite-GAN [43]. Christ *et al.* [35] proposed cascaded FCN architecture and dense 3D conditional random field (CRF) to automatically segment liver and liver lesions.

Since the GAN was proposed by Goodfellow *et al.* [44], it has shown great potential in the process of medical image analysis. For instance, Zhao *et al.* [43] proposed a Tripartite-GAN to synthesize liver contrast-enhanced MRI for liver tumors detection. Huo *et al.* [42] proposed a SynSeg-Net to perform segmentation tasks on the medical image without ground truth labels [Reference]. And Xu *et al.* [45] proposed a PSCGAN that simultaneously synthesizes an equivalent image of late-gadolinium-enhancement and segment the diagnosis-related tissues from cine MR images [Reference]. All these works demonstrated that GAN has great power in the field of medical image analysis.

The 2D model can not extract the depth information of the image sufficiently, so the segmentation accuracy is relatively low. On the other hand, 2.5D and 3D models need a lot of parameters, and they also have high requirements for hardware configuration. Limited resources limit the deep and complexity of 3D models. Meanwhile, with the deepening of CNNs, a new research problem arises: with information regarding input or gradient passes through multiple layers, it may disappear at the end (or beginning) of the network. Many recent publications have addressed this or related issues, many models, such as ResNets [28], Highway Networks [46], Densely Net [47], UNet [48], pass signals from one layer to the next through identity connections, creating short paths to allow better information and gradient flows. Therefore, we propose a nested system of Densely-UNet.

III. RADIOMICS-GUIDED DUN-GAN

Radiomics-guided DUN-GAN is the first to complete the accurate segmentation of lesions without CA in an innovative way. The framework consists of two adversarial networks: a DUN segmentor (Section III.A) and a Radiomics-guided discriminator (Section III.B)(as shown in Fig. 2). The two networks interact with each other.

A. DENSELY-U-CONNECTION SEGMENTOR

The segmentor includes a Dilated-Densely-Block(DDB) for extracting semantic feature, a global attention map extraction and guidance layer, and a U- Connection for sharing guidance information. 1) Dilated convolution extracts more detailed features by expanding the field of view, which better deals with low-contrast areas caused by non-contrast agents. 2) Dilated and Densely are combined (as shown in Fig. 3(a)) to better reduce the impact of gradient disappearance on the stability of the model. 3) New global attention model (GAM) (as shown in Fig. 3(b)) reveals advanced information and compensates for the pixel-level local features of the target in low-contrast images. That is, the segmentor replaces the convolution of the UNet with the DDB convolution block,

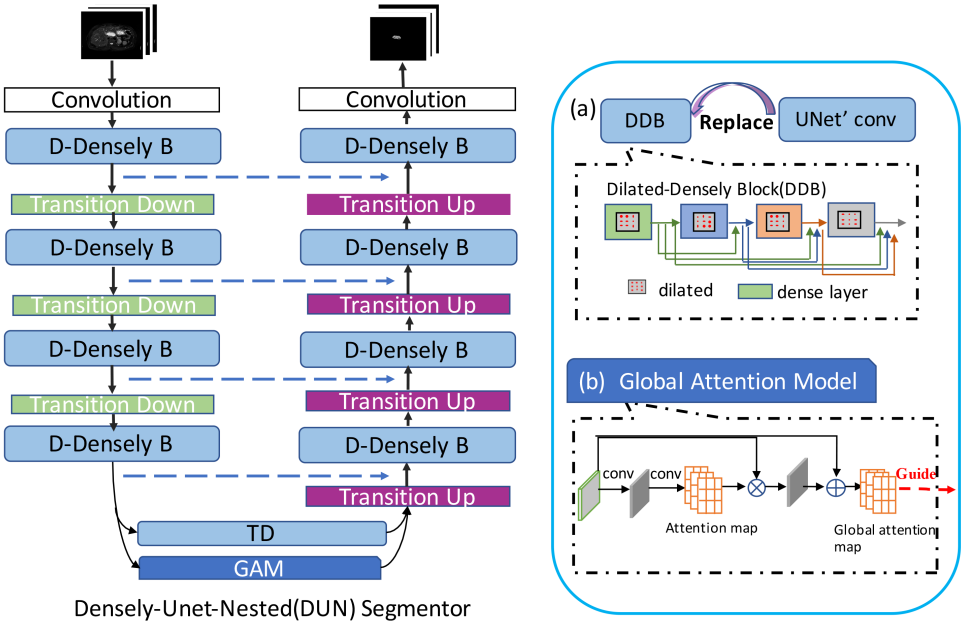

FIGURE 3. The structure of our Densely-U-Connection (DUN) Segmentor, which includes DDB, GAM, TD and TP. (a) DDB consists of Dilated Convolution and Dense layer. It goes through a series of operations of standard DilatedConv, BN, and ReLU activation functions. (b) The global connection added a global attention feature with guidance information to the network to guide the segmentation.

and innovatively nests two jump connection to form the DUN segmentor. Such a nested connection can both maximize the flow of information and share more details during the segmentation process, stably and accurately extracting ICR features with adversarial function.

1) SEMANTIC FEATURE EXTRACTION OF DILATED-DENSELY-BLOCK

The DenseNet has been proven to perform well in segmentation while significantly improving the flow of information between layers, so we use it as an extraction module for semantic features(as shown in Fig. 3(a)). Within each Dense block, the density connection method directly connects any layer to subsequent layers, thus avoiding repeated learning of features. Consequently, the ℓ^{th} layer receives the feature-maps of all preceding layers, $x_0, \ldots, x_{\ell-1}$ as input:

$$x_\ell = H_\ell\left([x_0, x_1, \ldots, x_{\ell-1}]\right) \tag{1}$$

The above $H_\ell(.)$ represents a non-linear transformation, which is a combined operation, which may contain a series of BN (Batch Normalization), ReLU, Pooling, and Conv operations.

Using Dilated convolution instead of traditional convolution to improve the feature extraction ability. Dilated convolution helps expand the receptive field, capturing a wider range of background information without reducing the resolution of the image or additional parameters. Finally, the receptive field is expanded, and the semantic features of the non-contrast image are extracted more efficiently. During the experiment, the dilation rate set to {1, 2, 4, 8} for each 3×3 kernel size. And, transition Down (TD) is a series of operations consisting of Conv, Batch Normalization (BN), ReLU, and Polling. Transition Up (TU)is the opposite operation of TD, consisting of DeConv, BN, and ReLU.

2) GLOBAL ATTENTION MODEL

Global attention model(GAM) enables the network to focus on the target region in a large image context. It reveals advanced information that compensates for pixel-level local features of objects in low-contrast images. Therefore, adding global attention feature maps as guidance information to the segmentor can improve the accuracy of segmentation. As shown in Fig. 3(b), an attention map is convoluted by two convolution layers, followed by the ReLU activation. In order to multiply attention map with the input feature map, we set the channel number of the first convolutional layer to half of the input image, and the channel number of the second convolutional layer is 1. We also use a residual connection in the attention module. Then the global attention feature maps are fused with local feature. The global attention feature map itself compensates for the local feature of the target and guides the decode path of UNet through providing guided information.

3) U-CONNECTION FOR SHARING GUIDANCE INFORMATION

UNet has been successfully applied in the segmentation field. It uses downsampling to gradually reduce the spatial resolution, while the upsampling process gradually increases the semantic dimension to recover the abstract image of the representation. The segmentor connects the layer information and the upsampled shared low-level information (for example, boundary information, discriminator competition

feedback information) through a U-skip connection, so that the decoder learns related information lost in the encoder. Finally, ICR features that compete with Radiomics-feature are learned, and image segmentation without CA is completed.

The parameter details and feature sizes for each layer of the DUN Segmentor as follows in Tab. 1.

TABLE 1. It shows the parameter details and feature sizes for each layer of the Densely-UNet-Nested (DUN) Segmentor. The DDB block mainly performs the feature extraction process, and the whole segmentation is completed by downsampling and upsampling of the TD and TU.

	Feature size	DUN Segmentor
input	256×256	
Conv 1	128×128	7×7, 48, stride 2
DDB 1	128×128	3×3,96, stride 2,dilation 2
TD layer 1	64×64	2×2 max plooling, 96
DDB 2	64×64	3×3,144, stride 2,dilation 2
TD layer 2	32×32	2×2 max plooling, 144
DDB 3	32×32	3×3,192, stride 2,dilation 2
TD layer 3	16×16	2×2 max plooling, 192
DDB 4	16×16	3×3,240, stride 2,dilation 2
TD layer 4	8×8	2×2 max plooling, 240
Global	8×8	GAM, 240
TU 1	16×16	2×2 upsampling, [3×3 DDB 4, dilation 2], 480
TU 2	32×32	2×2 upsampling, [3×3 DDB 3, dilation 2], 360
TU 3	64×64	2×2 upsampling, [3×3 DDB 2, dilation 2], 240
TU 4	128×128	2×2 upsampling, [3×3 DDB 1, dilation 2], 120
Conv= 2	128×128	1×1

B. RADIOMICS-GUIDED DISCRIMINATOR

The Radiomics-guided discriminator includes a semantic feature extraction model(SFEM), a Radiomics-feature extraction model(RFEM), and a Radiomics-guided Connection Layer (RgCL). Radiomics feature serves as guidance information, which guides the discriminator to extract more representative semantic features through RgCL. It can even guide the segmentor to learn the ICR feature through the adversarial mechanism. Finally, the mapping between images is learned and the accurate segmentation is completed.

1) SEMANTIC FEATURE EXTRACTION MODEL(SFEM)

To extract semantic feature extraction, classical image segmentation network VGG16 [27] is adopted. It uses several convolution layers with smaller convolution kernels to improve a convolution layer with larger convolution kernels. It reduces the parameters and carries out more non-linear mappings simultaneously, which improves and enhances the fitting expression ability of the network. The input of the semantic feature extraction network is the result of segmentor or ground truth image in 64×64 patch, and the output is the probability of the real or generated image. In the classic VGG16 frame, each layer of convolutional layer contains 2×4 convolution operations. The size of the convolution kernel is 3×3, the convolution step 1, the pooled kernel 2×2, the step size 2.

2) RADIOMICS-FEATURE EXTRACTION MODEL(RFEM)

Radiomics feature characterizes the microstructure and heterogeneity of the potential lesions [9]. The Radiomics feature is extracted and selected using the open-source platform-PyRadiomics [49], which uses several engineering hard-coded feature algorithms to process and extract radiological features from medical image data. Radiology utilizes data characterization algorithms for comprehensive and automated quantification of phenotypic features, such as shapes and textures, and reflects biological properties such as internal heterogeneity.

For each phase CE-MRI, Radiomics feature is characterized by micro -structure feature(M-feature) and heterogeneity feature(H-feature). M-feature was characterized using mesh surface, pixel, diameter and other shape features; H-feature was characterized using gray level co-occurrence matrix(GLCM), gray level-size zone matrix(GLSZM) and other texture features. PyRadiomics extracted radiological features for each lesion. The entire feature extraction process is completed by the radiomics feature extraction model(RFEM). In RFEM, the image and the corresponding mask image are input to the Pyradiomics platform. The platform characterizes the microstructure and heterogeneity of the lesion by extracting shape and texture features. PyRadiomics automatically selects the most important 75 features and performs data analysis on the features.

3) DISCRIMINATOR AFTER RgCL

RFEM extracts the Radiomics features (f_x, g_x and h_x) corresponding to the images of three-phase CE-MRI (T1-Delay, T1-ART and T1-PV). And SFEM extracts the semantic features V_x of segmented images or ground truth images. The features are reconnected and fully connected to form connectable vectors. At the same time, it is extracted and reshaped to extract 225 dimensions (75 each from T1-Delay, T1-ART and T1-PV). Mean, variance, skewness, and kurtosis were computed over the feature vectors within each lesion. Therefore, a total feature ($T_x = 225 \times 4$) were computed for each lesion. Finally, T_x and V_x are connected through Radiomics-guided Connection Layer (RgCL) to form Radiomics-guided fusion feature. After this feature is Softmax, the identification result is obtained. The whole process is shown in Fig. 4.

The guidance of Radiomics features consists of two parts: 1. Radiomics-guided fusion feature continuously optimizes VGG16 through discriminator loss function back propagation. Under the guidance of Radiomics, VGG16 performs parameter adjustment to extract the semantic features with characterization ability, thereby improving the identification ability. 2. Radiomics-guided fusion feature has stronger characterization ability, and can guide the work of the splitter through the confrontation mechanism(Fig. 4).

C. ADAPTIVE PIXEL-LEVEL-GUIDED HYBRID LOSS FUNCTION

The loss function contains discriminator loss $loss_D$ and segmentor loss $loss_S$. The overall losses are as follows:

$$\min_S \max_D L_{GAN}(S, D) = E_{y \sim p_{data}(y)} \left[\log D(y)\right] + E_{x \sim P_x(x)} \left[\log^{(1-D(S(x)))}\right] \quad (2)$$

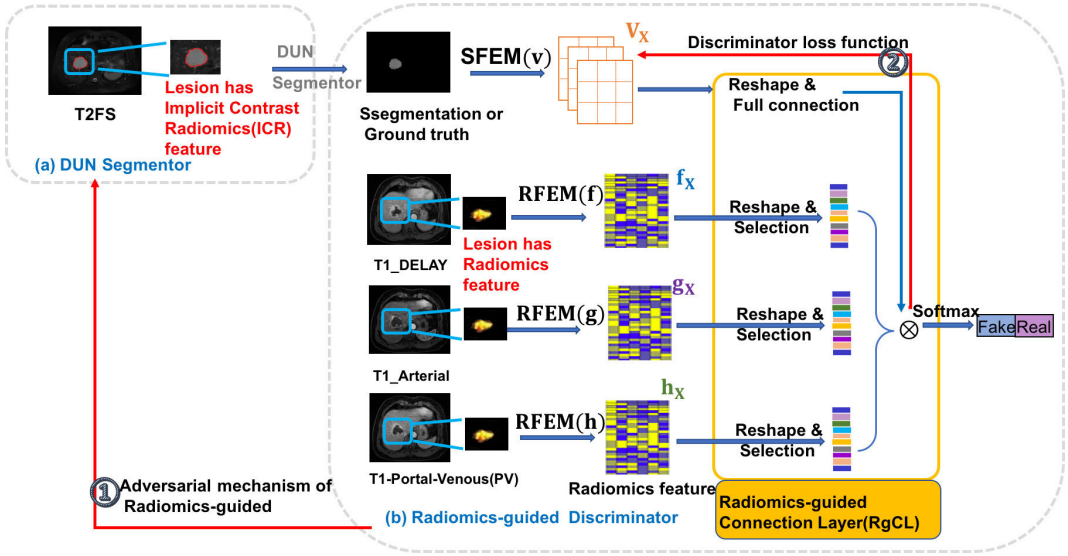

FIGURE 4. Radiomics-feature is used as a priori knowledge to identify and segment. 1. Under Radiomics-guided adversarial mechanism, Radiomics-feature guiding the extracting of more representative semantic features through the discriminator loss function. 2. It guides the extraction of implicit contrast radiomics (ICR) features in non-contrast images through the adversarial mechanism of Radiomics-guided.

Among them, input image x and its corresponding base fact y, and use x_i, y_i to represent the input and ground truth values at the pixel location, respectively.S tries to minimize this goal, while opponent D tries to maximize it.

In the game of GAN [44], the discriminator and segmentor are individually trained iteratively, so the objective function is also optimized separately. By competing, the two models are simultaneously enhanced, and follow the minimum-maximum game process. Firstly, the discriminator is optimized, and the $loss_D$ is as follows:

$$\begin{aligned} L_D &= \max_D L_{GAN}(S, D) \\ &= E_{y\sim p_{data}(y)}\left[\log D(y)\right] + E_{x\sim p_x(x)}\left[\log^{(1-D(S(x)))}\right] \end{aligned} \tag{3}$$

Among them, $E_{y\sim p_{data}(y)}$ represents the ground truth of segmentation, $E_{x\sim p_x(x)}$represents the predicted segmentation. D_y denotes the demotes the probability of the ground truth of segmentation and S_x denotes the predicted segmentation comes from our segmentor. The discriminating result is expected to be close to 1 during the training. For the generated sample, we want its discriminant results $D(S(x))$ to be closer to 0. Therefore, during training, the loss function adjusts the parameters of S to minimize $D(S(x))$ and the parameters of D to maximize $\log^{D(x)}$, and finally to balance the losses.

After completing the optimization of the discriminator model, it is necessary to achieve the optimization of the generated model. Existing work has proven that combining GAN losses with more traditional losses can effectively reduce ambiguity. Based on MICCAI, we use the generalized Jaccard instead of Dice index. On the one hand, Jaccard is differentiable and can be used to calculate backpropagation. On the other hand, it is a more appropriate distance measure relative to the Dice index. Therefore, we redefine the adaptive $loss_S$ function

$$\begin{aligned} L_S &= \min L_{GAN}(S, D) + w1 * L_{Jaccard}(S) \\ &\quad + w2 * L_{Pix\_CE}(S) \end{aligned} \tag{4}$$

$$\min L_{GAN}(S, D) = E_{x\sim p_x(x)}\left[\log^{(1-D(S(x)))}\right] \tag{5}$$

$$L_{Jaccard}(S) = -log\frac{|y \cap y_i| + \epsilon}{|y| + |y_i| - |y \cap y_i| + \epsilon} \tag{6}$$

$$L_{Pix\_CE}(S) = -\frac{1}{n\sum_x y\ln(a) + (1-y)\ln(1-a)} \tag{7}$$

The right side of Eqn(4) combines the traditional $loss_S$ with the Jaccard index and the pixel classification cross-entropy loss function, and automatically adjusts S by weighting parameters w1 and w2. First, in the optimization process, let the result of the discrimination D(S(x)) be close to 1, that is, let the total value be the smallest. Second, the weighting parameters w1 and w2 are a constant value indicating the weighting of the three losses. We solve equation (4) by alternately optimizing between S and D by using their respective loss functions. In Eqn(4), to prevent the denominator from being zero, we define ϵ as a very small number, using $\epsilon = 1 \times 10^{-15}$.

IV. EXPERIMENTAL STUDIES

A. DATA ACQUISITION

Our study data ultimately includes 250 subjects, 130 with an MRI-definitive typical appearance of a hemangioma, and 120 with a new untreated diagnosis of hepatocellular carcinoma(HCC). These data are provided after approval by the McGill University Health Centre. Participants provided written informed consent to participate in the study. All subjects underwent initial standard clinical liver MRI protocol

Algorithm 1 Radiomics-Guided DUN-GAN

Train

Input: Non-contrast MRI image x and its corresponding ground truth
mask of contrast-T1-Dealy MRI images y; Contrast-T1-Dealy MRI *Delay*;
Contrast-T1-Arterial MRI Art; Contrast-T1-Portal-Venous MRI PV;
The loss balanced weights w_1 and w_2; Initial learning rates lr_s and lr_d;
Mini-batch size n; The number of iterations T.

Output: Learned parameters Θ_{seg}, Θ_{dis}

1: Initialize the parameters Θ_{seg}, Θ_{dis} randomly and construct model;
2: for step in T do
3: Fed $x_n, y_n, Delay_n, Art_n$ and $PV_n \leftarrow x_n, y_n, Delay_n, Art_n$ and PV_n represent the x, y,*Delay*,Art and PV with mini-batch size n;
4: /* The forward propagation of $S(xn)$: */
5: $x_\ell = H_\ell([x_0, x_1, \ldots, x_{\ell-1}])$
6: $S(xn) = Densely - \text{Unet-Nested}S(x_l)$
7: /* The forward propagation of $D(\cdot)$: */
8: D(S(xn))=RgCL(VGG16($S(xn)$)+PyRadiomics($S(xn)$) + PyRadiomics($Delay_n$) + PyRadiomics(Art_n)+PyRadiomics(PV_n))
9: D(y(n))=RgCL(VGG16($D(y_n)$)+PyRadiomics($D(y_n)$) + PyRadiomics($Delay_n$)+PyRadiomics(Art_n) + PyRadiomics(PV_n))
10:/* The backward propagation of $S(x_n)$: */
11: $\Theta_{seg} = \Theta_{seg}\text{-}lr_s \bigtriangledown(L_S = \min L_{GAN}(S, D) + w_1 * L_{Jaccard}(\text{S}) + w_2 * L_{Pix\_CE}(\text{S}))$
12:/* The backward propagation of $D(\cdot)$: */
13: $\Theta_{dis} = \Theta_{dis}\text{-}lr_d \bigtriangledown L_D$
14:End for

Test

Input: Non-contrast MRI image x
Output: Segmentation result of x
1: /* The forward propagation of $S(xn)$: */
2: $x_\ell = H_\ell([x_0, x_1, \ldots, x_{\ell-1}])$
3: $S(xn) = Densely - \text{Unet-Nested}S(x_l)$
4:End

examinations with corresponding pre-contrast (T2FS [5mm; 256 × 256 px], diffusion-weighted images [6mm; 256 × 256 px], T1-Pre-contrast [4mm; 512 × 512px]), and contrast-enhanced images (arterial [4mm; 512 × 512 px], Portal-Venous [4mm; 512 × 512 px], late [4 mm; 512 × 512 px], 5-Min Delay [4mm; 512 × 512 px]) were collected after using gadolinium CA. Gadolinium contrast used in these protocols was gadobutrol 0.1 mmol/kg on a 3T MRI scanner (GE Signa). A radiologist with 7 years of experience in MR Liver imaging analyzed the three-phase CE-MRI and verified manual segmentations of the delayed in each scan as ground truth.

TABLE 2. Training configuration of the Radiomics-guided DUN-GAN. The parameters involved in the training process include the learning rate of the training model, batch size, optimization, and learning motivation.

Network Name	Segmentor	Discriminator
Training method	Stochastic Gradient Descent Optimizer	
Batch size	2	64
Initial learning rate	$e\times^{-3}$	$e\times^{-4}$
End learning rate	$e\times^{-6}$	$e\times^{-6}$
Learning momentum	0.9	

B. IMPLEMENTATION DETAILS

For training, the non-contrast T2FS images of 256 × 256 without cropping are instantly inputted into the segmentor. At the same time, all the input selected slices to the discriminator are directly resized to size 256 × 256. Among, ground truth (T1-delay images) of 512 × 512 need to directly manual adjusted to 256 × 256. And, the three-phase CE-MRI and the corresponding mask are also adjusted to 256 × 256. The setting of loss weight is described in section 3.3. Radiomics-guided DUN-GAN is implemented using the PyTorch package and MATLAB R2017a on a desktop computer with an Inter(R) CPU i5-6500 (3.19GHz). Because of its efficiency, the experiment uses a single NVIDIA GTX 1080 GPU with 8 GB of memory. The training configurations of the Radiomics-guided DUN-GAN are listed in Tab. 2. The network is optimized by a stochastic gradient descent method with a momentum of 0.9 and a weight attenuation of 0.005.

To evaluate the performance of our network, a standard ten-fold cross-validation is employed. Due to the limited data set, expanded 50 data based on 200 data sets of MICCAI, and simple data enhancements were performed, including horizontal flip, vertical flip, and 90^o, 180^o, 270^o rotation. Ten-fold cross-validation ensures that all images are used for training and testing, and each image is only used for testing once. Our method does not involve any post-processing at any stage.

C. CONFORMANCE ASSESSMENT

We evaluate the consistency between our algorithm and expert manual segmentation through the following indicators.

1) THREE MEASURES

In this study, the evaluation of the segmentation results of liver lesions mainly uses those three measures [50]: Dice similarity coefficient (DSC), Precision and Recall. The results of the calculation of the lesion segmentation results for each test data are compared with the ground truth. Among, Precision and Recall indicators are calculated based on the confusion matrix [51]. The elements of the i-th row and the j-th column of the confusion matrix represent the number of images with predicted grade i and ground truth grade j. The concrete equality is as follows:

1) Dice Similarity Coefficient(DSC). The DSC calculation formula is:

$$DSC = \frac{2 \times |Seg \cap Ref|}{|Seg| + |Ref|} \times 100 \tag{8}$$

Among them, *Seg* is the result of algorithm segmentation, and *Ref* is the result of ground truth. The DSC value is close to 1, the more accurate the lesion segmentation result is. On the contrary, the segmentation result does not substantially coincide with the gold standard, and the detection of lesions fails, or the segmentation error occurs.

2) Precision. The precision calculation formula is:

$$Precision = \frac{TP}{TP + FP} \times 100 \tag{9}$$

Among them, *TP* is Truth Positive that the classification results are consistent with the ground and belong to positive samples. *FP* is False Positive that classification result is inconsistent with the gold standard, and the negative samples are divided into positive samples. Precision refers to the ratio between the number of positive samples correctly classified and the number of all positive The value is close to 1 means the less the negative sample is misclassified into positive samples.

3) Recall. The Racall calculation formula is:

$$Recall = Sensitivity = \frac{TP}{TP + FN} \times 100 \tag{10}$$

Recall refers to the ratio of the number of positive samples correctly classified to the number of all positive samples. The value is close to 1, the fewer positive samples are misclassified into negative samples.

Precision and recall rate are mutually influential. Generally, high accuracy leads to low recall rate and low Precision leads to high recall rate. In practice, the Precision and recall rate should be kept as high as possible. In practical applications, the Accuracy and recall rate should be as high as possible.

2) ROC CURVE AND PR CURVE

The Receiver Operating Characteristic (ROC) curve and the Precision-Recall (PR) curve are drawn from the confusion matrix, which is used to evaluate the classification performance of the machine learning algorithm for a given data set. ROC curve, which combines sensitivity and specificity by graphic method, can accurately reflect the relationship between specificity and sensitivity of the method and is a comprehensive representation of test accuracy. The more convex the ROC curve is, the closer it is to the upper left corner, which indicates that the diagnostic value of ROC curve is greater. The Area Under Curve (AUC) can evaluate diagnostic accuracy. PR curve combines recall rate and accuracy with the graphic method, which can accurately reflect the relationship between them. The PR curve is to the upper right corner, the greater its diagnostic value. ROC and PR curves are relatively simple and intuitive. The clinical accuracy of the analysis method can be observed by graphics and can be directly judged by the naked eye.

V. EXPERIMENTAL RESULTS AND EVALUATION

Radiomics-guided DUN-GAN is the first to complete the segmentation of liver lesions without contrast agents. The segmentation results can prove that our results outperform other methods, and the best result with a DSC of 93.47± 0.83 is obtained. The results verify that the Radiomics-guided DUN-GAN is accurate and robust, and it has the possibility of becoming a safe, inexpensive and time-saving medical assistant tool in clinical diagnosis.

A. QUALITATIVE EVALUATION RESULTS OF RADIOMICS-GUIDED DUN-GAN

1) SEGMENTATION RESULTS

Fig. 5 shows that Radiomics-guided DUN-GAN outperforms other networks inaccurate image segmentation without CA. In Fig. 5, the first row represents the type of lesion that can be observed in the non-contrast image. In the process of segmentation, the boundary of the lesion is missed because the contrast between the boundary of the lesion and the surrounding organs is low, and the complete segmentation is more complicated. The second line represents the type of lesion that is barely visible in the original image. There is a big gap between the results of segmentation. Compared with other methods, our method has a significant improvement. It can extract the features of the lesion better and complete the segmentation. Besides, as shown in Fig. 5 (a), our segmentation result has the highest overlap with ground truth, representing the most accurate segmentation. In non-contrast images(T2FS), visible lesions in non-contrast images are marked with red lines. In DEC-MRI images, the radiologist marked the lesion as a ground truth with a red line and marked the lesion area with green. (a) shows the segmentation results of different models. Green is ground truth and red is the result of segmentation. The larger the overlap area between red and green, the better the segmentation result.

2) VISUALIZATION OF MULTI-PHASE RADIOMICS-FEATURE

Fig. 6 shows the visualization results of Radiomics-feature corresponding to the multi-phase DCE-MRI of three different subjects extracted by RFEM. It was evident that the characteristics of different subjects are quite different, and the characteristics of different phases of the same subject are also very different. As shown in the blue box, for subject 1, the GLSZM feature is more obvious in the PV phase, and the shape feature is more obvious in Art. The characteristics of the three different phases can play a complementary role. After RgCL fusion, it can contain more features that can characterize the lesion and improve the discriminatory ability. At the same time, multi-phase radiomics feature is more helpful for segmentor to extract M- and H- features in non-contrast images, that is, ICR features. It can also improve the guidance of the segmentor.

3) QUALITATIVE VISUALIZATION OF FEATURE MAPS

In order to clearly see the specific contribution of multi-phase Radiomics feature, Fig. 7 shows the feature maps of Radiomics-guided DUN-GAN without Radiomics feature, Radiomics-guided DUN-GAN with Radiomics feature of

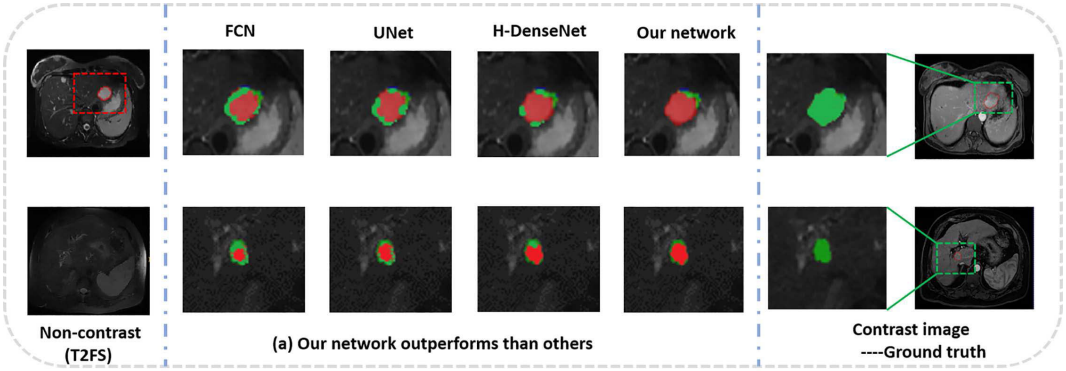

FIGURE 5. Qualitative visualization shows that Radiomics-guide DUN-GAN outperforms other networks, which can accurately segment different types of lesions in non-contrast MRI images. (a) Four columns show the segmentation results of FCN, UNet, H-DenseNet and our method respectively. Green represents ground truth, and red represents the result of segmentation. The bigger the overlapping area, the more accurate the segmentation result is. Although some lesions can hardly be seen in non-contrast images, our network achieves accurate segmentation.

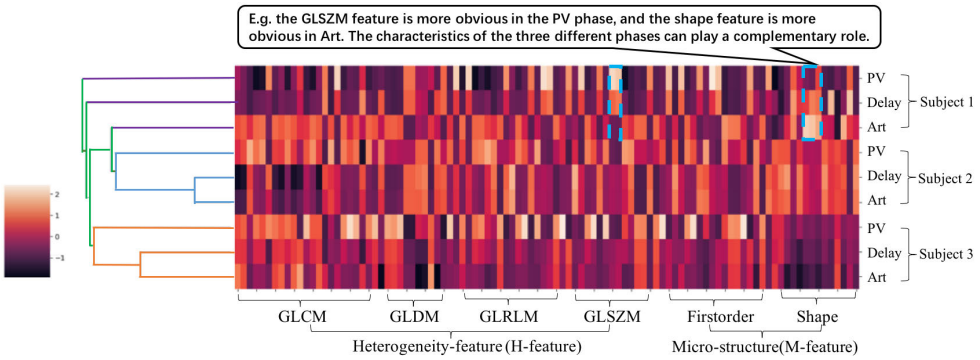

FIGURE 6. Radiomics-feature visualization results of different phases corresponding to the three subjects. The abscissa is the feature of Radiomics-feature. H-features include gray level co-occurrence matrix (GLCM), gray level dependence matrix (GLDM), gray level run length matrix (GLRLM) and gray level size zone matrix (GLSZM) class feature, and M features include firstorder and shape class feature. Each block represents the result of the corresponding feature, and the color represents the corresponding different values.

T1-Delay (MICCAI 2019), and our Radiomics-guided DUN-GAN with multi-phase Radiomics-feature, respectively. We can see the Radiomics feature enhances the M feature extraction (especially for the shape feature extraction) by comparing the yellow arrow in the feature maps. And, we can see the Radiomics feature enhances the H feature extraction (especially for the texture feature extraction) by comparing the red arrow in the feature maps.

In the first line (without radiomics-guided) of Fig. 7, most of the edge features may be lost because of the low contrast between the lesion and the organ in the non-contrast MRI. In the second line (with radiomics-guided of T1-Delay), ICR features extracted by the segmentor are also partially miss, because the single-phase T1-Delay contains much fewer shape features than the fusion features of multi-phase DCE-MRI. At the same time, the last two columns of Fig. 7 show the segmentation results and zoomed local patches of the tumor area. The red line is ground-truth, the green line is the tumor area displayed on the non-contrast image, and the yellow line is the result of the Radiomics-guided DUN-GAN segmentation. DCE-MRI images contain richer and more obvious Radiomics-feature, which means more distinct shapes and texture. It demonstrates that multi-phase radiomics-feature is input to the discriminator as a priori knowledge, which helps segmentor to extract key implicit contrast radiomics (ICR) in non-contrast images via adversarial learning. So that under radiomics-guided mechanism, the Radiomics-guided DUN-GAN improves the accuracy of liver lesions segmentation on non-contrast MRI.

B. QUANTITATIVE PERFORMANCE EVALUATION

We compare the segmented lesion results with the ground truth noted by expert radiologists, which show that our method can provide lesion segmentation automatically and accurately. Our method achieved best results with overall DSC is 93.47± 0.83, with an accuracy of 96.23 and a recall rate of 91.79. As shown in Fig. 8 (a) (b), the ROC curve is close to the upper left corner, and AUC is close to 1, which represents the accuracy of the test is very high. The PR curve is near the upper right corner, which represents the better performance of the network. At the same time, In Fig. 8, the combined-feature (Radiomics-guided

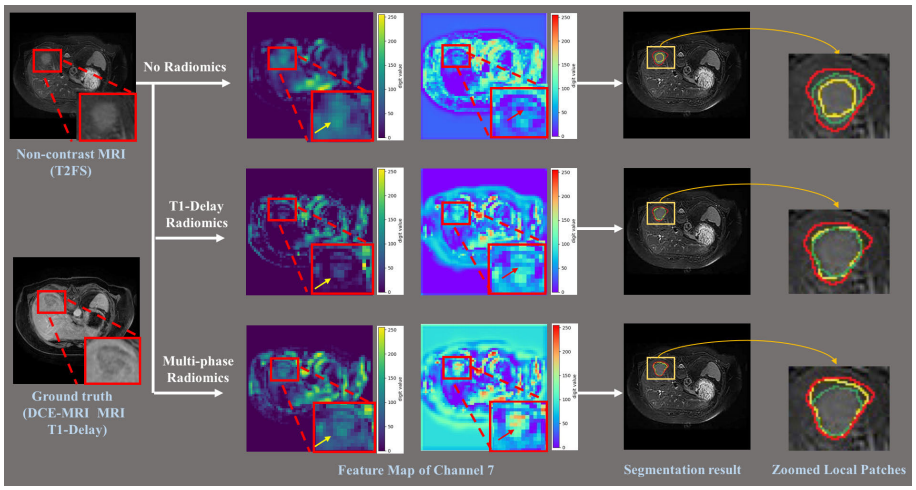

FIGURE 7. Examples of Non-contrast MRI segmentation. The yellow arrow in the feature maps represents the difference of M-feature between Radiomics-guided DUN-GAN without Radiomics, Radiomics-guided DUN-GAN with T1-Delay radiomics and our Radiomics-guided DUN-GAN. The red arrow in the feature maps represents the difference of H-feature between Radiomics-guided DUN-GAN without Radiomics, Radiomics-guided DUN-GAN with T1-Delay radiomics and our Radiomics-guided DUN-GAN. The last two columns show the segmentation results and zoomed local patches of the tumor area. It demonstrates that Radiomics-guided DUN-GAN can improve the accuracy of segmentation on non-contrast MRI.

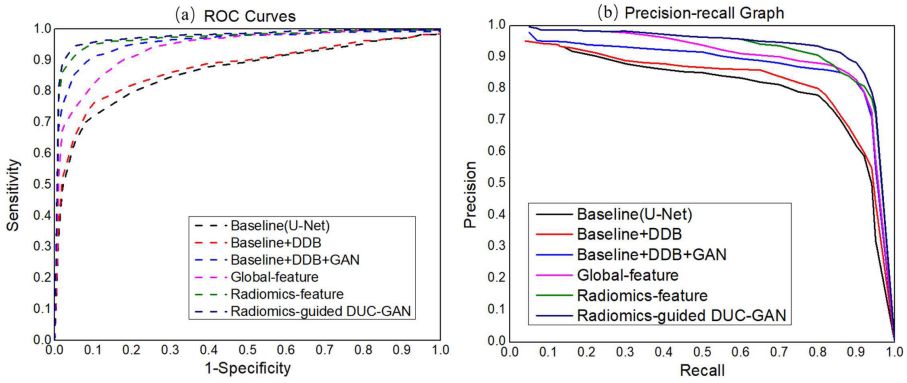

FIGURE 8. The ROC and PR values of our method are superior to other modules. (a) and (b) show the ROC and PR of the segmentation results of the different modules, respectively. ROC and PR are consistent, indicating that Radiomics feature and global attention features can improve the accuracy of our approach.

DUN-GAN) network yields higher ROC and PR values than using Radiomics-feature or Global-feature alone, Section 5.3.2 will analyze in detail.

C. ABLATION EXPERIMENTS

1) COMPARISON OF DIFFERENT MODEL OF RADIOMICS-GUIDED DUC-GAN

In this section, we compare and evaluate the methods presented (In Section 3.2) through several experiments. According to Section 3, it is proposed to add the Radiomics feature as a guide to the discriminator, using the adversarial mechanism to guide the learning of the segmentor. At the same time, global attention features are proposed to embed more semantic information into the fusion features based on MICCAI. We proposed DDB based on UNet to improve the stability of the network. To prove the validity of our method, we tested their performance separately(as shown in Tab. 3).

The result of UNet segmentation is taken as a baseline during the experiment, and the segmentation result directly for the non-contrast image was 73.21 $\pm$0.62. (1) On this basis, DDB was added (the second row in Tab. 3), and DSC increased from 73.21 $\pm$0.62 to 75.69 $\pm$ 0.34. Although the value of improvement is small, the experiment shows that the network can converge quickly. The results show that DDB can extract more detailed features and thus help to improve the segmentation. Dense connection changes the way of network connection and improves the convergence of the network. (2) On this basis, the GAN network was added (the third row in the Tab. 3), and the DSC value increased from

TABLE 3. Liver lesion without CA segmentation Dice scores of our method achieved the best result. Comparing the results of ablation experiments with those of Baseline, the results can intuitively show that each module proposed in our method is effective.

Model	DSC
Baseline(U-Net)	73.21 ±0.62
Baseline + DDB	75.69 ± 0.34
Baseline + DDB + GAN	83.65 ± 0.51
Baseline + DDB + GAN with Global-feature	87.81±0.72
Baseline + DDB + GAN with Radiomics-feature	92.17±0.79
Radiomics-guided DUN-GAN	**93.47± 0.83**

75.69 ± 0.34 to 83.65 ± 0.51. This shows that the adversarial mechanism can effectively extract the key features of the image without CA, which helps correct segmentation. Therefore, the combination of DUN segmentor network and adversarial module makes the Radiomics-guided DUN-GAN network a more effective solution to segment lesions in non-contrast images.

Tab. 3 shows that the four innovations (adversarial mechanism of multi-phase Radiomics-guided, nested structure of DDB, direction strategy of multi-integrate-feature, and adaptive hybrid loss function) have an excellent performance in improving segmentation. It makes Radiomics-guided DUN-GAN model achieve the best DSC of 93.47± 0.83.

2) COMPARISON OF DIFFERENT FEATURE OF RADIOMICS-GUIDED DUN-GAN

Tab. 3 also demonstrates the effectiveness of the guided fusion features of Radiomics-feature and Global-feature. The segmentation result of Radiomics-guided DUN-GAN with 93.47± 0.83 as the baseline (sixth row in Tab. 3). (1) If the Radiomics-feature is removed, the segmentation result decreases from 93.47± 0.83 to 87.81±0.72, which indicates that Radiomics-feature can characterize the key features in the non-contrast image, which is the key to improve the segmentation. (2) If the Global-feature is removed, the segmentation result is reduced from 93.47± 0.83 to 92.17±0.79, which indicates that Global-feature can reveal advanced information that can compensate for pixel-level local features of the target in low-contrast images without CA.

In the comparative experiment with 250 data sets, the Radiomics-feature guidance network, the Global-feature guidance network, and the Combined-feature-directed network were trained separately using ten-fold cross-validation. Fig.8(a) (b) shows ROC and PR with different characteristics. The ROC curve of combined-feature is closest to the upper left corner and the PR curve is closest to the upper right corner. Fig.8 visually shows the results of network segmentation guided by different features through the values of DSC, Precision, Sensitivity and Specificity. The DSC value is consistent with Tab. 3.

Besides, Fig. 9 demonstrates that our proposed new feature-to-relationship learning strategy can effectively integrate multiple features. The results of Precision, Sensitivity and Specificity are arranged in the order of Combined-feature Radiomics-feature, Global attention feature (Global feature). Combined-feature and Radiomics-feature have significantly

TABLE 4. Results were summarizing different effects of our proposed method with different loss. Based on GAN, ablation study was conducted separately. It is verified that our loss function improves the accuracy of segmentation.

Model	GAN	GAN+Jaccard	GAN+Pix	GAN+Jaccard+Pix	Proposed
DSC	88.67±0.61	91.43±0.75	91.95±0.19	92.82±0.43	**93.47± 0.83**

improved results than Global-feature, which demonstrates that the inclusion of Radiomics-feature can well characterize lesions and guide segmentation. Besides, although the result of combined-feature is only 0.84 better than the Radiomics-feature, this is of great significance in the segmentation without CA. Therefore, under the guidance of Radiomics-feature, the ability of the network to extract the features after fusion of global features with low-level and high-level features is improved. Through confrontation, fusion and mutual guidance, the features that can characterize the lesions in non-contrast images are finally learned. The results show that under a reasonable model, effective features can guide the model to extract more critical features, which is an effective scheme to improve the segmentation results.

3) COMPARISON OF DIFFERENT LOSS FUNCTION OF RADIOMICS-GUIDED DUN-GAN

Tab. 4 proves that our proposed pixel classification cross-entropy loss function is more conducive to the segmentation of non-contrast images. Eqn. (1) is the loss function of the segmentor. Based on GAN's adversarial training, DSC increased by 2.76 under Jacquard's training. Because the Jaccard coefficient is differentiable, it facilitates the calculation of the back propagation of the loss function and reduces the overfitting of the network. Pixel classification cross-entropy loss function training improved DSC by 3.28. Because pixel cross loss can effectively solve the problem of class imbalance. The innovative pixel-level-guided hybrid loss function is innovatively proposed to be 0.65 higher than the ordinary combination. The weighting parameters and the weights that balance the three losses can increase the convergence speed of the network and help improve the segmentation performance.

D. COMPARISON WITH STATE-OF-ART MODEL

Existing state-of-art methods rely on enhanced public data sets, such as an open platform of Digital human liver database by the affiliated hospital of Qingdao University, Liber Lesion Segmentation Challenge (LiTS) by 2017 MICCAI Public Challenge. LiTS dataset contains 201 contrast-enhanced abdominal CT scans. Using the LiTS dataset, Li *et al.* [41] designed a DenseUnet to effectively detect intra-slice features of liver and lesion segmentation and proposed an H-DenseUnet framework to explore the hybrid features of liver and lesion segmentation. This method obtains the lesion segmentation result with 82.4. Chlebus *et al.* [52] used UNet with random forest to get the DSC with 65 and Han [37] used Res-UNet to get the DSC with 67. Three popular networks (FCN, UNet, ResNets) and two cutting edge representative segmentation methods using GANs

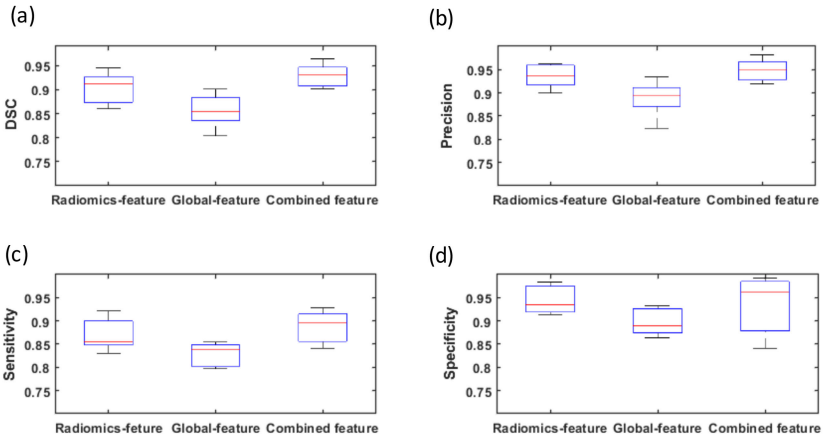

FIGURE 9. Using the Combined feature to have better results than other features. (a)-(d) show the DSC, Precision, Sensitivity, and Specificity of the model segmentation under the guidance of different features, which show that the combined feature has the best results.

TABLE 5. The results of the different methods for the segmentation of the data set (non-contrast + contrast) verify the validity of our method.

Model	Non-contrast/Contrast	DSC
FCN	Contrast	75.92±0.48
	Non-contrast	68.43±0.72
UNet	Contrast	85.42±0.29
	Non-contrast	73.21±0.54
ResNet	Contrast	84.37±0.7
	Non-contrast	71.24±0.81
Res-UNet	Contrast	90.37±0.41
	Non-contrast	79.41±0.65
H-DenseUNet	Contrast	91.31±0.37
	Non-contrast	80.72±0.81
SynSeg-Net	Contrast	91.84±0.91
	Non-contrast	83.95±0.75
PSCGAN	Contrast	92.19±0.69
	Non-contrast	85.17±0.49
Our Method	**Non-contrast**	**93.47± 0.83**

(SynSeg-Net [42], and PSCGANs [45]) are tested using our data sets (non-contrast image, T2FS and contrast-enhanced image, delay-DE images) verify the validity of the models. The results are shown in Tab. 5.

Tab. 5 demonstrates that our method has completed the accurate segmentation lesion of non-contrast MRI images and can be an effective tool for clinical diagnosis in the future. Tab. 5 shows that for the same network, the results of using MRI images are higher than those of using CT images in the paper, which proves that contrast-enhanced MRI is the best imaging method for cancer detection and differential diagnosis [53], [54]. Simultaneously, the segmentation result of the MRI contrast-enhanced image is higher than non-contrast image because the CA makes the boundary of the lesion clear. Compared to an enhanced CT or MRI, a non-contrast MRI is easy to perform, requires less acquisition time, has no need for contrast media (i.e., lower costs and no side effects compared to enhanced MRI), has no associated radiation hazard, and is relatively inexpensive. Han [55] has proved that Non-contrast MRI may have the potential for the surveillance of HCC. The 12th row of Tab. 5 shows that PSCGAN has better results in MRI image segmentation than other existing methods. Although our method is to segment the image without CA, the result is 1.28 higher than that of other best results 92.19 using CA image.

VI. CONCLUSION

In this paper, we developed Radiomics-guided DUN-GAN that segments liver lesions in non-contrast MRI images for the first time. Radiomics-guided DUN-GAN includes a DUN segmentor and a Radiomics-guided discriminator. In the DUN segmentor, DDB nested structure to improve information flow, DUN extracts the more accurate feature under direction strategy of multi-integration feature. Thus, the DUN segmentor completes the segmentation of liver lesions in non-contrast MRI images through extracting key implicit contrast radiomics (ICR) features in non-contrast images. In the Radiomics-guided discriminator, multi-phase Radiomics feature input discriminator to improve the ability of discriminators as prior guidance features. Moreover, it uses the adversarial mechanism to guide the extraction of multiple features of the segmentor. Through the images of 250 clinical subjects, Radiomics-guided DUN-GAN obtained the Dice Similarity Coefficient (DSC) results of 93.47± 0.83 for the segmentation of lesions in non-contrast images. The results verify that the Radiomics-guided DUN-GAN is accurate and robust, and it has the possibility of becoming a safe, inexpensive and time-saving medical assistant tool in clinical diagnosis.

REFERENCES

[1] A. Radtke, S. Nadalin, G. C. Sotiropoulos, E. P. Molmenti, T. Schroeder, C. Valentin-Gamazo, H. Lang, M. Bockhorn, H. O. Peitgen, C. E. Broelsch, and M. Malago, "Computer-assisted operative planning in adult living donor liver transplantation: A new way to resolve the dilemma of the middle hepatic vein," *World J. Surg.*, vol. 31, no. 1, p. 175, 2007.

[2] J. Chapiro, R. Duran, M. Lin, R. E. Schernthaner, Z. Wang, B. Gorodetski, and J.-F. Geschwind, "Identifying staging markers for hepatocellular carcinoma before transarterial chemoembolization: Comparison of three-dimensional quantitative versus Non–three-dimensional imaging markers," *Radiology*, vol. 275, no. 2, pp. 438–447, May 2015.

[3] C. B. Sirlin, H. K. Hussain, E. Jonas, M. Kanematsu, J. M. Lee, E. M. Merkle, M. Peck-Radosavljevic, S. B. Reeder, J. Ricke, and M. Sakamoto, "Consensus report from the 6th international forum for liver MRI using gadoxetic acid," *J. Magn. Reson. Imag.*, vol. 40, no. 3, pp. 516–529, Sep. 2014.

[4] E. A. Sadowski, L. K. Bennett, M. R. Chan, A. L. Wentland, A. L. Garrett, R. W. Garrett, and A. Djamali, "Nephrogenic systemic fibrosis: Risk factors and incidence estimation," *Radiology*, vol. 243, no. 1, pp. 148–157, Apr. 2007.

[5] F. Stacul, A. J. van der Molen, P. Reimer, J. A. W. Webb, H. S. Thomsen, S. K. Morcos, T. Almén, P. Aspelin, M.-F. Bellin, O. Clement, and G. Heinz-Peer, "Contrast induced nephropathy: Updated ESUR contrast media safety committee guidelines," *Eur. Radiol.*, vol. 21, no. 12, pp. 2527–2541, Dec. 2011.

[6] J. Llovet, M. Ducreux, R. Lencioni, A. Di Bisceglie, P. Galle, and J. Dufour, "European association for the study of the liver European organisation for research and treatment of cancer: EASL-EORTC clinical practice guidelines: Management of hepatocellular carcinoma," *J. Hepatol.*, vol. 56, no. 4, pp. 908–943, 2012.

[7] J.-Y. Choi, J.-M. Lee, and C. B. Sirlin, "CT and MR imaging diagnosis and staging of hepatocellular carcinoma: Part I. Development, growth, and spread: Key pathologic and imaging aspects," *Radiology*, vol. 272, no. 3, pp. 635–654, Sep. 2014.

[8] C. Xu, L. Xu, Z. Gao, S. Zhao, H. Zhang, Y. Zhang, X. Du, S. Zhao, D. Ghista, H. Liu, and S. Li, "Direct delineation of myocardial infarction without contrast agents using a joint motion feature learning architecture," *Med. Image Anal.*, vol. 50, pp. 82–94, Dec. 2018.

[9] R. Shiradkar, S. Ghose, I. Jambor, P. Taimen, O. Ettala, A. S. Purysko, and A. Madabhushi, "Radiomic features from pretreatment biparametric MRI predict prostate cancer biochemical recurrence: Preliminary findings," *J. Magn. Reson. Imag.*, vol. 48, no. 6, pp. 1626–1636, Dec. 2018.

[10] X. Xiao, J. Zhao, Y. Qiang, J. Chong, X. Yang, N. G.-F. Kazihise, B. Chen, and S. Li, "Radiomics-guided gan for segmentation of liver tumor without contrast agents," in *Proc. Int. Conf. Med. Image Comput. Comput.-Assist. Intervent.* Berlin, Germany: Springer, 2019, pp. 237–245.

[11] D. Kainmüller, T. Lange, and H. Lamecker, "Shape constrained automatic segmentation of the liver based on a heuristic intensity model," in *Proc. MICCAI Workshop 3D Segmentation Clinic, A Grand Challenge*, 2007, pp. 109–116.

[12] R. Beichel, C. Bauer, A. Bornik, E. Sorantin, and H. Bischof, "Liver segmentation in CT data: A segmentation refinement approach," in *Proc. MICCAI Workshop 3D Segmentation Clinic, Grand Challenge*. Berlin, Germany: Springer, 2007, pp. 235–245.

[13] A. Bornik, R. Beichel, E. Kruijff, B. Reitinger, and D. Schmalstieg, "A hybrid user interface for manipulation of volumetric medical data," in *Proc. 3DUI*, vol. 6, Mar. 2006, pp. 29–36.

[14] A. Beck and V. Aurich, "Hepatux—A semiautomatic liver segmentation system," in *Proc. MICCAI Workshop 3D Segmentation Clinic, Grand Challenge*. Berlin, Germany: Springer, 2007, pp. 225–233.

[15] B. M. Dawant, R. Li, B. Lennon, and S. Li, "Semi-automatic segmentation of the liver and its evaluation on the MICCAI 2007 grand challenge data set," in *3D Segmentation The Clinic: A Grand Challenge*, 2007, pp. 215–221.

[16] J. Lee, N. Kim, H. Lee, J. B. Seo, H. J. Won, Y. M. Shin, and Y. G. Shin, "Efficient liver segmentation exploiting level-set speed images with 2.5 D shape propagation," in *Proc. MICCAI Workshop 3-D Segmentat. Clinic, Grand Challenge*, 2007, pp. 189–196.

[17] A. Wimmer, G. Soza, and J. Hornegger, "Two-stage semi-automatic organ segmentation framework using radial basis functions and level sets," in *Proc. MICCAI Workshop 3D Segmentation Clinic, Grand Challenge*. Berlin, Germany: Springer, 2007, pp. 179–188.

[18] P. Slagmolen, A. Elen, D. Seghers, D. Loeckx, F. Maes, and K. Haustermans, "Atlas based liver segmentation using nonrigid registration with a b-spline transformation model," in *Proc. MICCAI Workshop 3D Segmentation Clinic, Grand Challenge*. Berlin, Germany: Springer, 2007, pp. 197–202.

[19] G. Sethi, B. S. Saini, and D. Singh, "Segmentation of cancerous regions in liver using an edge-based and phase congruent region enhancement method," *Comput. Electr. Eng.*, vol. 53, pp. 244–262, Jul. 2016.

[20] S. Patil, V. R. Udupi, and D. Patole, "A robust system for segmentation of primary liver tumor in CT images," *Int. J. Comput. Appl.*, vol. 75, no. 13, pp. 6–10, Aug. 2013.

[21] A. Baâzaoui, W. Barhoumi, A. Ahmed, and E. Zagrouba, "Semi-automated segmentation of single and multiple tumors in liver CT images using entropy-based fuzzy region growing," *IRBM*, vol. 38, no. 2, pp. 98–108, Apr. 2017.

[22] A. Hoogi, C. F. Beaulieu, G. M. Cunha, E. Heba, C. B. Sirlin, S. Napel, and D. L. Rubin, "Adaptive local window for level set segmentation of CT and MRI liver lesions," *Med. Image Anal.*, vol. 37, pp. 46–55, Apr. 2017.

[23] M. K. T. N. Amarajothi and S. Manikandan, "Liver tumor segmentation using single level set method with shape and intensity prior," *Int. J. Appl. Eng. Res.*, vol. 10, no. 20, p. 2015, 2015.

[24] W. Huang, Y. Yang, Z. Lin, G.-B. Huang, J. Zhou, Y. Duan, and W. Xiong, "Random feature subspace ensemble based extreme learning machine for liver tumor detection and segmentation," in *Proc. 36th Annu. Int. Conf. IEEE Eng. Med. Biol. Soc.*, Aug. 2014, pp. 4675–4678.

[25] X. Zhang, J. Tian, D. Xiang, X. Li, and K. Deng, "Interactive liver tumor segmentation from ct scans using support vector classification with watershed," in *Proc. Annu. Int. Conf. IEEE Eng. Med. Biol. Soc.*, Aug. 2011, pp. 6005–6008.

[26] C.-L. Kuo, S.-C. Cheng, C.-L. Lin, K.-F. Hsiao, and S.-H. Lee, "Texture-based treatment prediction by automatic liver tumor segmentation on computed tomography," in *Proc. Int. Conf. Comput., Inf. Telecommun. Syst. (CITS)*, Jul. 2017, pp. 128–132.

[27] A. Krizhevsky, I. Sutskever, and G. E. Hinton, "ImageNet classification with deep convolutional neural networks," in *Proc. Adv. Neural Inf. Process. Syst.*, 2012, pp. 1097–1105.

[28] K. He, X. Zhang, S. Ren, and J. Sun, "Deep residual learning for image recognition," in *Proc. IEEE Conf. Comput. Vis. Pattern Recognit. (CVPR)*, Jun. 2016, pp. 770–778.

[29] J. Long, E. Shelhamer, and T. Darrell, "Fully convolutional networks for semantic segmentation," in *Proc. IEEE Conf. Comput. Vis. Pattern Recognit. (CVPR)*, Jun. 2015, pp. 3431–3440.

[30] S. Albarqouni, C. Baur, F. Achilles, V. Belagiannis, S. Demirci, and N. Navab, "AggNet: Deep learning from crowds for mitosis detection in breast cancer histology images," *IEEE Trans. Med. Imag.*, vol. 35, no. 5, pp. 1313–1321, May 2016.

[31] H. Chen, Q. Dou, L. Yu, J. Qin, and P.-A. Heng, "VoxResNet: Deep voxelwise residual networks for brain segmentation from 3D MR images," *NeuroImage*, vol. 170, pp. 446–455, Apr. 2018.

[32] P. Moeskops, M. A. Viergever, A. M. Mendrik, L. S. de Vries, M. J. N. L. Benders, and I. Isgum, "Automatic segmentation of MR brain images with a convolutional neural network," *IEEE Trans. Med. Imag.*, vol. 35, no. 5, pp. 1252–1261, May 2016.

[33] A. A. A. Setio, F. Ciompi, G. Litjens, P. Gerke, C. Jacobs, S. J. van Riel, M. M. W. Wille, M. Naqibullah, C. I. Sanchez, and B. van Ginneken, "Pulmonary nodule detection in CT images: False positive reduction using multi-view convolutional networks," *IEEE Trans. Med. Imag.*, vol. 35, no. 5, pp. 1160–1169, May 2016.

[34] A. Ben-Cohen, I. Diamant, E. Klang, M. Amitai, and H. Greenspan, "Fully convolutional network for liver segmentation and lesions detection," in *Deep Learning and Data Labeling for Medical Applications*. Berlin, Germany: Springer, 2016, pp. 77–85.

[35] P. F. Christ, M. E. A. Elshaer, F. Ettlinger, S. Tatavarty, M. Bickel, P. Bilic, M. Rempfler, M. Armbruster, F. Hofmann, M. D'Anastasi, and W. H. Sommer, "Automatic liver and lesion segmentation in ct using cascaded fully convolutional neural networks and 3d conditional random fields," in *Proc. Int. Conf. Med. Image Comput. Comput.-Assist. Intervent.* Springer, 2016, pp. 415–423.

[36] C. Sun, S. Guo, H. Zhang, J. Li, M. Chen, S. Ma, L. Jin, X. Liu, X. Li, and X. Qian, "Automatic segmentation of liver tumors from multiphase contrast-enhanced CT images based on FCNs," *Artif. Intell. Med.*, vol. 83, pp. 58–66, Nov. 2017.

[37] X. Han, "Automatic liver lesion segmentation using a deep convolutional neural network method," 2017, *arXiv:1704.07239*. [Online]. Available: http://arxiv.org/abs/1704.07239

[38] Q. Zhu, B. Du, B. Turkbey, P. Choyke, and P. Yan, "Exploiting interslice correlation for MRI prostate image segmentation, from recursive neural networks aspect," *Complexity*, vol. 2018, pp. 1–10, Feb. 2018.

[39] Q. Dou, H. Chen, Y. Jin, L. Yu, J. Qin, and P.-A. Heng, "3D deeply supervised network for automatic liver segmentation from CT volumes," in *Proc. Int. Conf. Med. Image Comput. Comput.-Assist. Intervent.* Berlin, Germany: Springer, 2016, pp. 149–157.

[40] Q. Zhu, B. Du, J. Wu, and P. Yan, "A deep learning health data analysis approach: Automatic 3D prostate MR segmentation with densely-connected volumetric ConvNets," in *Proc. Int. Joint Conf. Neural Netw. (IJCNN)*, Jul. 2018, pp. 1–6.

[41] X. Li, H. Chen, X. Qi, Q. Dou, C.-W. Fu, and P.-A. Heng, "H-DenseUNet: Hybrid densely connected UNet for liver and tumor segmentation from CT volumes," *IEEE Trans. Med. Imag.*, vol. 37, no. 12, pp. 2663–2674, Dec. 2018.
[42] Y. Huo, Z. Xu, H. Moon, S. Bao, A. Assad, T. K. Moyo, M. R. Savona, R. G. Abramson, and B. A. Landman, "SynSeg-Net: Synthetic segmentation without target modality ground truth," *IEEE Trans. Med. Imag.*, vol. 38, no. 4, pp. 1016–1025, Apr. 2019.
[43] J. Zhao, D. Li, Z. Kassam, J. Howey, J. Chong, B. Chen, and S. Li, "Tripartite-GAN: Synthesizing liver contrast-enhanced MRI to improve tumor detection," *Med. Image Anal.*, vol. 63, Jul. 2020, Art. no. 101667.
[44] I. Goodfellow, J. Pouget-Abadie, M. Mirza, B. Xu, D. Warde-Farley, S. Ozair, A. Courville, and Y. Bengio, "Generative adversarial Nets," in *Proc. Adv. Neural Inf. Process. Syst.*, 2014, pp. 2672–2680.
[45] C. Xu, L. Xu, P. Ohorodnyk, M. Roth, B. Chen, and S. Li, "Contrast agent-free synthesis and segmentation of ischemic heart disease images using progressive sequential causal GANs," *Med. Image Anal.*, vol. 62, May 2020, Art. no. 101668.
[46] R. K. Srivastava, K. Greff, and J. Schmidhuber, "Training very deep networks," in *Proc. Adv. Neural Inf. Process. Syst.*, 2015, pp. 2377–2385.
[47] G. Huang, Z. Liu, L. Van Der Maaten, and K. Q. Weinberger, "Densely connected convolutional networks," in *Proc. IEEE Conf. Comput. Vis. Pattern Recognit. (CVPR)*, Jul. 2017, pp. 4700–4708.
[48] O. Ronneberger, P. Fischer, and T. Brox, "U-net: Convolutional networks for biomedical image segmentation," in *Proc. Int. Conf. Med. Image Comput. Comput.-Assist. Intervent.* Berlin, Germany: Springer, 2015, pp. 234–241.
[49] J. J. M. van Griethuysen, A. Fedorov, C. Parmar, A. Hosny, N. Aucoin, V. Narayan, R. G. H. Beets-Tan, J.-C. Fillion-Robin, S. Pieper, and H. J. W. L. Aerts, "Computational radiomics system to decode the radiographic phenotype," *Cancer Res.*, vol. 77, no. 21, pp. e104–e107, Nov. 2017.
[50] T. Heimann *et al.*, "Comparison and evaluation of methods for liver segmentation from CT datasets," *IEEE Trans. Med. Imag.*, vol. 28, no. 8, pp. 1251–1265, Aug. 2009.
[51] W. J. Niessen, C. J. Bouma, K. L. Vincken, and M. A. Viergever, "Error metrics for quantitative evaluation of medical image segmentation," in *Performance Characterization in Computer Vision*. Berlin, Germany: Springer, 2000, pp. 275–284.
[52] G. Chlebus, H. Meine, J. H. Moltz, and A. Schenk, "Neural network-based automatic liver tumor segmentation with random forest-based candidate filtering," 2017, *arXiv:1706.00842*. [Online]. Available: http://arxiv.org/abs/1706.00842
[53] N. Snowberger, S. Chinnakotla, R. M. Lepe, J. Peattie, R. Goldstein, G. B. Klintmalm, and G. L. Davis, "Alpha fetoprotein, ultrasound, computerized tomography and magnetic resonance imaging for detection of hepatocellular carcinoma in patients with advanced cirrhosis," *Alimentary Pharmacol. Therapeutics*, vol. 26, no. 9, pp. 1187–1194, Aug. 2007.
[54] A. Rode, B. Bancel, P. Douek, M. Chevallier, V. Vilgrain, G. Picaud, L. Henry, F. Berger, T. Bizollon, J.-L. Gaudin, and C. Ducerf, "Small nodule detection in cirrhotic livers: Evaluation with US, spiral CT, and MRI and correlation with pathologic examination of explanted liver," *J. Comput. Assist. Tomogr.*, vol. 25, no. 3, pp. 327–336, May 2001.
[55] S. Han, J.-I. Choi, M. Y. Park, M. H. Choi, S. E. Rha, and Y. J. Lee, "The diagnostic performance of liver MRI without intravenous contrast for detecting hepatocellular carcinoma: A case-controlled feasibility study," *Korean J. Radiol.*, vol. 19, no. 4, pp. 568–577, 2018.

XIAOJIAO XIAO received the M.D. degree in computer science and technology from the Taiyuan University of Technology, China, in 2017, where she is currently pursuing the Ph.D. degree in image processing. Her recent research interests include medical image processing and the deep learning.

YAN QIANG received the Ph.D. degree from the Department of Computer Application Technology, Taiyuan University of Technology (TYUT), China, in November 2010. He is currently working as a Professor with the Department of Computer Science and Technology, TYUT. His recent research interest includes data mining, mainly working on image processing and cloud computing.

JUANJUAN ZHAO received the Ph.D. degree from the Department of Computer Application Technology, Taiyuan University of Technology (TYUT), China, in November 2010. She is currently working as a Professor with the Department of Computer Science and Technology, TYUT. Her recent research interests include medical image processing and deep learning.

XINGYU YANG received the B.S. degree in computer science and technology from the Taiyuan University of Technology (TYUT), China, in 2020, where he is currently pursuing the M.S. degree in medical image processing.

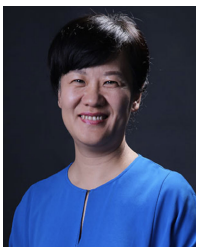

XIAOTANG YANG received the Ph.D. degree from the Department of Computer Application Technology, Taiyuan University of Technology (TYUT), China, in November 2010. She is currently working as a Professor with Shanxi Medical University and the Vice President of Shanxi Cancer Hospital, China. Her recent research interests include breast and body tumor imaging diagnosis and related scientific research.